International Journal of Nanomedicine

Dovepress
open access to scientific and medical research

Open Access Full Text Article

ORIGINAL RESEARCH

pH- and Ultrasound-Responsive Paclitaxel-Loaded Carboxymethyl Chitosan Nanodroplets for Combined Imaging and Synergistic Chemoradiotherapy

This article was published in the following Dove Press journal:
International Journal of Nanomedicine

Mengmeng Shang[1]
Xiao Sun[1]
Lu Guo[1]
Dandan Shi[1]
Ping Liang[2]
Dong Meng[1]
Xiaoying Zhou[1]
Xinxin Liu[1]
Yading Zhao[1]
Jie Li[1]

[1]Department of Ultrasound, Qilu Hospital of Shandong University, Jinan 250012, People's Republic of China; [2]Department of Interventional Ultrasound, Chinese PLA General Hospital, Beijing 100853, People's Republic of China

Background: Synergistic chemoradiotherapy (CRT) has become a primary effective curative approach for many solid cancers. However, CRT is still associated with several obstacles, including the increases in side effects and systemic toxicity. Incorporating nanocarriers into CRT is a new and exciting approach to solve these obstacles. The purpose of the present study was to design a unique pH- and ultrasound-responsive perfluoropentane-encapsulated, paclitaxel (PTX)-loaded carboxymethyl chitosan nanodroplets (NDs) for combined imaging and synergistic CRT.

Materials and Methods: The NDs were prepared by a homogenization/emulsion method. Their physicochemical properties, echogenicity and biocompatibility were evaluated. PTX-loaded NDs with a high loading efficiency and encapsulation efficiency were prepared and their pH-responsive drug release profile was determined by dialysis sack method. Then, PC3 cells were exposed to (1) PTX (4 μg/mL), (2) NDs (30 μg/mL), (3) PTX-loaded NDs (34 μg/mL), (4) RT (6 Gy), (5) RT (10 Gy), (6) combination of PTX (4 μg/mL), ultrasound (0.5 W/cm^2, 30 s) and RT (6 Gy), (7) combination of NDs (30 μg/mL), ultrasound (0.5 W/cm^2, 30 s) and RT (6Gy), (8) combination of PTX-loaded NDs (30 μg/mL), ultrasound (0.5 W/cm^2, 30 s) and RT (6 Gy). 24 hrs later, CCK-8 assay, flow cytometry and migration assay were carried out to evaluate their therapeutic effects in CRT.

Results: The desired NDs were successfully prepared, which were with round, spherical shapes, relatively smooth surfaces, core-shell structures and uniform in sizes (<300 nm with PDI<0.3 when at pH≧6.0). The NDs exhibited good abilities in pH-dependent charge conversion, biocompatibility and ultrasound contrast echogenicity. The in vitro drug release from PTX-loaded NDs (the highest loading efficiency and encapsulation efficiency were 20.35% and 91.58%) was pH dependent and exhibited an initial burst followed by a sustained drug release. The results of the CCK-8 assay, flow cytometry and migration assay all showed PTX-loaded NDs combined ultrasound and RT significantly enhanced cell responses in CRT.

Conclusion: The pH- and ultrasound-responsive PTX-loaded NDs, which exhibited a high echogenicity, drug delivery ability and radiosensitization ability, could be a feasible option for combined imaging and novel enhancing approach in synergistic CRT.

Keywords: nanodroplets, ultrasound contrast agents, chemoradiotherapy, radiosensitizer, paclitaxel, chitosan

Correspondence: Jie Li
Department of Ultrasound, Qilu Hospital of Shandong University, 107 Wenhua Xi Road, Jinan 250012, People's Republic of China
Tel +86-531-82166101
Fax +86-531-86927544
Email jieli301@163.com

Introduction

Chemoradiotherapy (CRT), which refers to the synergistic administration of chemotherapy and radiotherapy (RT), now plays an important role in cancer oncology.[1,2]

submit your manuscript | www.dovepress.com
DovePress
http://doi.org/10.2147/IJN.S233669

The main rationale of CRT is provoked to be an increasing therapeutic effect of RT by drug-induced sensitization of tumor tissue.[2] Significant evidence has existed supporting the use of CRT as a primary effective curative approach for many solid cancers, such as head and neck, esophageal, lung, pancreatic and prostate cancers.[3–7] Even though CRT might be favored by many physicians, aggressive therapy is still associated with several obstacles, including the increases in side effects and systemic toxicity.[8,9] Hence, much advancements are in urgent need to further improve the therapeutic efficacy and reduce the overall toxicity of the treatment.

Considering the benefits of nanomedicine, a new and exciting approach is to incorporate a nanotechnology-based strategy into CRT to both promote the antitumor effect and reduce the systematic toxicity.[10] Nanotechnology is an emerging and promising field that uses nanocarriers to provide various benefits in cancer diagnosis and therapy.[11–14] Nanocarrier drug delivery systems (DDSs) are particularly well suited for cancer applications owing to their targeting and controlled release capability[15] and due to the phenomenon of enhanced permeability and retention (EPR).[16] Many investigators have reported the capabilities of various nanocarriers in the synergistic CRT. For example, one strategy involves the use of biocompatible PLGA-PEG nanoparticles (NPs) co-delivered with paclitaxel (PTX) and cisplatin to enhance CRT efficiency in lung cancer.[17] In another approach, alginate hydrogel network with cisplatin and AuNPs co-loaded was used to enhance CRT efficiency in colon adenocarcinoma.[18]

Different from the other kinds of nanocarriers extensively investigated so far, few studies have focused on the use of nanoscale ultrasound contrast agents (UCAs) as therapeutic agents in CRT. As a matter of fact, nanoscale UCAs can not only deliver anticancer agents to the targeted site, but also enhance the uptake of agents with the help of ultrasound irradiation.[19] What's more, nanoscale UCAs have been demonstrated to be a potential precise and visualization therapy for cancer management.[20] Therefore, the nanoscale UCAs, which are capable of delivering the anticancer or radiosensitization agents and possess ultrasound imaging ability, are desired to provide competitive advantages of high efficiency and low toxicity in CRT. In addition, considering the specific microenvironment of solid tumors (including low extracellular pH, hypoxia, high interstitial fluid pressure),[21] the nanoscale UCAs should better be designed with stimuli-responsive property to benefit from passive targeting mechanisms.

To achieve the proof-of-principle, the PTX-loaded carboxymethyl chitosan (CMC) nanodroplets (NDs), which have a homogeneous nanoscale-sized structure for combined ultrasound imaging and CRT, were prepared in this study. The liquid-phase perfluoropentane (PFP), an ultrasound-responsive gas precursor, was encapsulated in the NDs. The human prostate cancer cell line PC3 was used as a disease model in vitro. A series of experiments were carried out to evaluate the physicochemical properties, pH-responsive charge conversion ability, echogenicity as UCAs, biocompatibility, drug release property, cell targeting ability and therapeutic effects in CRT.

Materials and Methods

Materials

CMC (molecular weight 100–300 kDa, degree of deacetylation 90%, degree of carboxymethylation 95%) was purchased from Santa Cruz Biotechnology (TX, USA). Tween 20, lecithin, PTX and 0.1% crystal violet stain solution were purchased from Solarbio Sciences and Technology (Beijing, China). PFP (C_5F_{12}, min. 98%) was purchased from J&K Scientific Ltd. (Beijing, China). RPMI-1640, phosphate-buffered saline (PBS, pH 7.4), 0.25% trypsin-EDTA, fetal bovine serum (FBS) and antibiotics (penicillin 100U/mL and streptomycin 100mg/mL) were purchased from Gibco Company (NY, USA). Cell counting kit-8 (CCK-8) was from Sigma-Aldrich (MO, USA). Annexin V-FITC apoptosis detection kit with PI was from BD Biosciences, Pharmingen (San Diego, USA). All other chemicals and solvents were obtained commercially as analytical-grade reagents and used as received without further purification or treatment.

Cell Line

The human prostate cancer cell line PC-3 was acquired from Cheeloo College of Medicine, Shandong University (Shandong, China). The use of the cell line in this study was approved by the Research Ethics Committee of Qilu Hospital of Shandong University. Cells were cultured in RPMI-1640 medium containing 10% FBS and 1% antibiotics and maintained in CO_2 incubator at 37°C with 98% humidity and 5% CO_2 environment.

Preparation and Characterization of NDs

In order to introduce echogenic property into the final NDs, PFP which has a boiling point of 29.2°C was formulated into the NDs by oil in water (O/W) emulsification method. In brief, a fixed-ratio mixture of PFP (as oil

phase), Tween 20 and lecithin were homogenized in deionized water for 2 min at 15,000 rpm using FJ2000-S homogenizer (Shanghai, China) under the ice bath condition. Then, CMC solution (0.2% w/v) (as water phase) was added dropwise into the emulsion and homogenized for another 2 min. After centrifugation at 500 rpm for 3 min, the upper solution was collected and finally filtered through a 0.45 μm filter (Millipore, MA, USA). The ND sample solution was allowed to store at 4°C for 2 h in rubber-capped vial to prevent vaporization. Before in vitro cellular experiments, the ND sample solution was centrifuged at 15,000 rpm for 5 min at 4°C using an analytical ultracentrifuge (J-26XP; Beckman Coulter, Inc., CA, USA). Then, the sediment representing the desired NDs was washed 3 times with sterile 0.9% saline solution and redissolved in a certain volume of 0.9% saline solution to give a final concentration gradient.

To determine the size and polydispersity of the ND populations, the ND sample solution was firstly observed with a bright-field microscope at 400× and 1000× magnifications (OLYMPUS BX41, Olympus Corporation, Tokyo, Japan). Scanning electron microscopy (SEM) (EVOMA 10, Zeiss, Jena, Germany) and transmission electron microscopy (TEM) (JEM-1011, JEOL, Tokyo, Japan) were used to visualize the morphology and structure of the ND populations. Samples were prepared by placing 50 μL of the ND sample solution on a 300-mesh copper grid and drying at room temperature.

In addition, the pH of the ND sample solution was adjusted to four different pH values (7.4, 6.8, 6.0 and 5.0) by the addition of specified amounts of 0.1 mol/L HCl. Each pH value corresponded to a single experiment that allowed investigating the impact of pH gradient on the ND size, distribution range, polydispersity index (PDI) and zeta potential, which were measured with a Zetasizer Nano ZS90 analyzer (Malvern Instruments Ltd., Worcestershire, UK).

Ultrasound Imaging

In order to assess the echogenicity of the ND sample, an in vitro acoustic test was performed by exposing the NDs to a medical beam as shown in Figure 1. Briefly, the ND sample solution was injected into a plastic pipette (with an inner diameter of 1 cm) submerged in a water tank containing 800 mL degassed, deionized water in a thermostatic bath set to 25°C and 37°C. The contents of the tank were maintained with stirring to agitate the NDs. The NDs were incubated in the water tank for 20 min before the medical beam exposure. A clinical ultrasound system (LOGIQ E9; GE, USA) was used with a 9 L linear transducer. The greyscale imaging process was selected with a center frequency of 9.0 MHz and

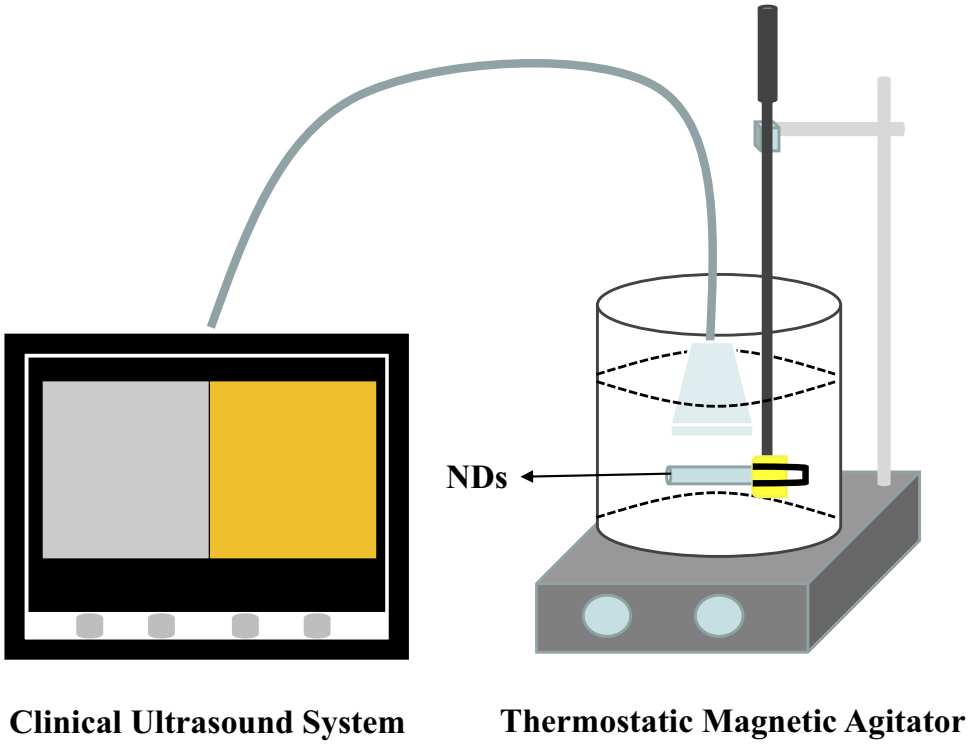

Figure 1 Setup to monitor the echogenicity of NDs as UCAs for ultrasound imaging.

different mechanical index (MI) series (0.5, 0.9, and 1.2). The focal zone was placed at the center of the sample. Five images of each sample were acquired. The greyscale level of the pixels within the region of interest (ROI) on the sample, which was normalized to that of the degassed, deionized water, was quantitatively calculated by image J 1.46r. The contrast enhancements were monitored using a contrast mode from 0 min to 10 min with a center frequency of 9.0 MHz, transmit power of 80% and a dynamic range of 60 dB. To verify whether the ND sample could be destroyed using the medical beam, it was burst three times at the time point of 11 min with a "manual flash" module. All the images were recorded as dynamic imaging files for consecutive analysis. The contrast intensity was analyzed via the ROI technique using "Q analysis" software of the ultrasound system. The contrast intensity of the ND samples was normalized to that of the degassed, deionized water. Survival ratio (SR) was calculated as the contrast intensity at each time point/the maximum contrast intensity×100%. All experiments were conducted in triplicate.

In vitro Cytotoxicity of NDs on PC3 Cell Line

Cell viability was chosen as a cytotoxicity parameter and determined using the CCK8 assay. Briefly, PC3 cells in the exponential growth phase were seeded in 96-well plates at a density of 1×10^4 cells/well. After 24 h of growth, treatments with various concentrations of NDs were applied to the cell wells. Then, the cells were incubated at 37°C with 5% CO_2 humidified atmosphere. After incubating for another 24 h, the medium containing the ND sample was discarded and replaced with fresh medium (100 μL) containing 10 μL of CCK-8 solution. And the cells were subsequently cultured for 1.5 h. After gentle agitation for 1 min, an Infinite F200 multimode plate reader (Tecan, Männedorf, Switzerland) was used to detect the absorbance of each well at 450 nm. All experiments were conducted in triplicate.

Hemolysis Assay

The hemolysis assay was approved by the Research Ethics Committee of Qilu Hospital of Shandong University. The blood donor's written informed consent was obtained before the assay. The hemolysis assay was achieved according to the modified method of Staedler et al.[22] 5 mL fresh human blood in sodium heparin-containing tubes was obtained from leftovers of analytical blood with normal values. The blood cells were separated by centrifugation of whole blood dilution in sterile 0.9% saline solution at 1200 rpm for 10 min and then washed three times. The desired blood cells were resuspended in 12 mL sterile 0.9% saline solution. For the hemolysis experiment, blood cell suspension (100 μL) was treated with 5 mL of ND suspension at a certain indicated concentration. The 0.9% saline solution was used as a negative control (0% hemolysis), and the deionized water was used as a positive control (100% hemolysis). All the samples were incubated for 1 h at 37°C and the mixture was centrifuged at 1200 rpm for 5 min. The separated supernatant containing hemoglobin released from the lysed RBCs was measured at 545 nm using an Infinite F200 multimode plate reader (Tecan, Männedorf, Switzerland). All experiments were conducted in triplicate. The hemolytic rate of the samples was calculated as the following equation:

$$\text{Hemolytic rate } (\%) = (OD_{sample} - OD_{negative}) / (OD_{positive} - OD_{negative})$$

Preparation and Optimization of PTX-Loaded NDs

For anticancer therapy, PTX-loaded NDs were also prepared with a certain amount of PTX mixing into the CMC solution (0.2% w/v) using the same method for drug-free NDs. The drug loading efficiency (LE) and encapsulation efficiency (EE) were measured according to the modified method of Xu et al.[23] The PTX-loaded ND solution sample was centrifuged at 15,000 rpm for 5 min at 4°C using an analytical ultracentrifuge (J-26XP; Beckman Coulter, Inc., CA, USA). The supernatant was analyzed by an ultraviolet (UV) spectrophotometer (Shimadzu UV-1800, Japan) at 230 nm using a calibration curve. The LE and EE were calculated using the following equation:

$$LE = M_0 / M_{CS} \times 100\%$$

$$EE = M_0 / M_{PTX} \times 100\%$$

Here, M_0 refers to the weight of PTX enveloped in the NDs, M_{CS} refers to the weight of CMC added in the system, M_{PTX} refers to the weight of PTX added in the system.

Finally, the optimized formula of preparing PTX-loaded NDs was determined according to the LE and EE.

pH-Responsive Drug Release from PTX-Loaded NDs

In vitro pH-responsive drug release profile of PTX-loaded NDs was determined by the dialysis sack method. Briefly,

about 2 mg drugs equivalent to the PTX-loaded ND solution were transferred into a dialysis bag (molecular weight cut-off 3500, Sigma, MO, USA) and incubated in 50 mL PBS (with pH 7.4, 6.8, 6.0 and 5.0, respectively) and shaken in an incubation shaker (TS-100C, Shanzhi instrument equipment company, Shanghai, China) set at 37°C and 100 rpm. The drug release study had been done for 72 h. At a certain time interval, 1 mL filtrate was collected for analysis and replaced with 1 mL fresh buffer. The amount of released PTX was determined by the UV spectrophotometer method using a calibration curve. The accumulative drug release rate was calculated using the following equation:

$$\text{Accumulative release of PTX } (\%) = M_t/M_0 \times 100\%$$

Here, M_t is the amount of PTX released after time t, and M_0 is the amount of PTX initially encapsulated in the NDs.

Cell Targeting Study of PTX-Loaded NDs on PC3 Cell Line

For cell targeting studies, PC3 cells in the exponential growth phase were seeded in 6-well plates at a density of 3×10^5 cells/well and incubated overnight for attachment. After attachment, the cells were treated with fresh medium (with pH of 6.8) containing a certain amount of PTX-loaded NDs for 2 h. At the end of incubation time, the medium was discarded and the wells were washed with PBS 3 times. Then, the cell images were captured using a microscope at 400× magnifications (OLYMPUS BX41, Olympus Corporation, Tokyo, Japan).

Groups and Treatments

PC3 cells in the exponential growth phase were seeded in 6-well plates at a density of 3×10^5 cells/well and incubated for 24 h. Then, these PC3 cells were randomly divided into 9 groups: Control group (incubated with normal medium, without therapeutic ultrasonic irradiation and radiation exposure), PTX group (incubated with medium containing PTX, without therapeutic ultrasonic irradiation and radiation exposure), ND group (incubated with medium containing NDs, without therapeutic ultrasonic irradiation and radiation exposure), PTX-NDs group (incubated with medium containing PTX-loaded NDs, without therapeutic ultrasonic irradiation and radiation exposure), RT (6 Gy) group (incubated with normal medium, radiation exposure with dose of 6 Gy), RT (10 Gy) group (incubated with normal medium, radiation exposure with dose of 10 Gy), PTX+RT (6 Gy)+US group (therapeutic ultrasonic irradiation at 1.5 h after incubation with medium containing PTX, then radiation exposure with dose of 6 Gy), NDs +RT (6 Gy)+US group (therapeutic ultrasonic irradiation at 1.5 h after incubation with medium containing NDs, then radiation exposure with dose of 6 Gy), PTX-NDs+RT (6 Gy)+US group (therapeutic ultrasonic irradiation at 1.5 h after incubation with medium containing PTX-loaded NDs, then radiation exposure with dose of 6 Gy) (Note: US =ultrasound). Here, the concentration of PTX was 4 μg/mL (the IC_{50} of PTX to PC3 cells at 24 h was determined as 6.292 μg/mL, with 95% CI [4.789 μg/mL, 8.265 μg/mL] by CCK8 assay), the concentration of NDs was 30 μg/mL, the concentration of PTX-NDs (the concentration of the PTX enveloped in these NDs equivalent to 4 μg/mL) was 34 μg/mL. The ultrasonic irradiation was performed with a therapeutic ultrasound device (US10, Cosmogamma Corporation, Italy), the parameters were set as follows: fixed frequency of 1 MHz, duty cycle of 70%, pulse repetition rate of 100 Hz, sound intensity of 0.5 W/cm^2 and irradiation time of 30 s. Cells exposed to radiation were irradiated with 6 Gy or 10 Gy using a medical linear accelerator (Varian 23 EX, Varian medical system, USA) using a 160-KVp source, at 25 mAmp and an average dose rate of 100 cGy/min. Radiation dose and rate were calculated empirically.

After the given various treatments, the PC3 cells were incubated for another 24 h for the following assays.

In vitro Cytotoxicity Assay

Cell viability was measured using the CCK8 assay. These PC3 cells were washed with PBS 3 times and then harvested separately. The cells were seeded in 96-well plates at a density of 2×10^4 cells/well and incubated overnight for attachment. The medium in the wells was discarded and replaced with a fresh medium (100 μL) containing 10 μL of CCK-8 solution. And the cells were subsequently cultured for 1.5 h. After gentle agitation for 1 min, an Infinite F200 multimode plate reader (Tecan, Männedorf, Switzerland) was used to detect the absorbance of each well at 450 nm. All experiments were conducted in triplicate.

Flow Cytometry Assay

Flow cytometry (Beckman Coulter, Miami, USA) with annexin V-FITC/PI double staining was used to explore the cell apoptosis. In brief, at the end of the given treatment period, these PC3 cells were removed by 0.25% trypsinization, centrifuged and washed with ice-cold PBS

for 3 times. Then, the cells in each tube (at least 1×10^4 cells) were resuspended with 100 μL ice-cold 1× binding buffer and stained with a total of 5 μL FITC and 5 μL PI. Then, cells were incubated for 15 min at room temperature in the dark. At last, 400 μL ice-cold 1× binding buffer was added. The data were analyzed using FlowJo software (version 7.6.1, USA). All experiments were conducted in triplicate.

Cell Migration Assay

The migration assay was performed using Transwell chambers (Corning, Lowell, MA, USA) in a 24-well plate. For each group, 5×10^4 cells in 200 μL FBS-free medium were placed in the upper part of each chamber, whereas 600 μL medium containing 20% FBS was added to the bottom wells as a chemoattractant. 24 h later, the chambers were removed and then fixed with methyl alcohol for 15 min, stained with 0.1% crystal violet solution for 30 min. The migratory cells were counted in 5 random fields per insert under a microscope at 20× magnification. All experiments were conducted in triplicate.

Statistical Analysis

The data discussed above were presented as mean±SD. Statistical significance of differences was derived using *t*-tests, one-way ANOVA analysis with Bonferroni post-tests. All statistical analyses were performed using the SPSS software (version 13.0; SPSS Inc, Chicago, IL). A p value<0.05 was considered statistically significant.

Results

ND Characterization

NDs consisting mainly of a CMC shell and a PFP core were successfully prepared by a homogenization/emulsion method in this study (Figure 2).

The microscopy, SEM and TEM images of NDs are presented in Figure 3. The NDs were round, spherical shapes with relatively smooth surfaces, core-shell structures and uniform in sizes and had less aggregation.

The sizes, PDI values and zeta potentials of NDs at different pH conditions are illustrated in Figure 4. Figure 4A and B showed that when the pH value was over 6.0, the NDs showed no significant difference in

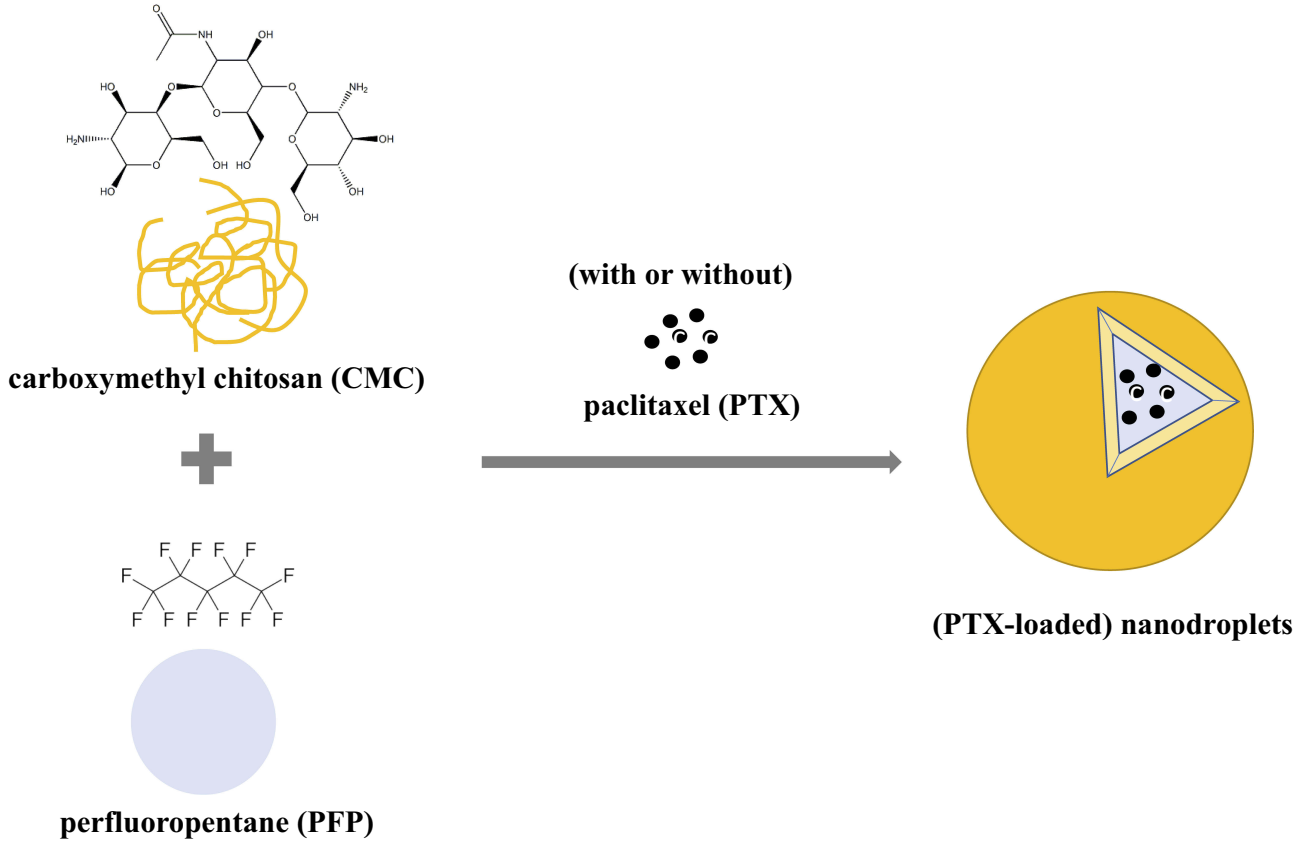

Figure 2 Schematic illustration of NDs (with or without PTX loaded).

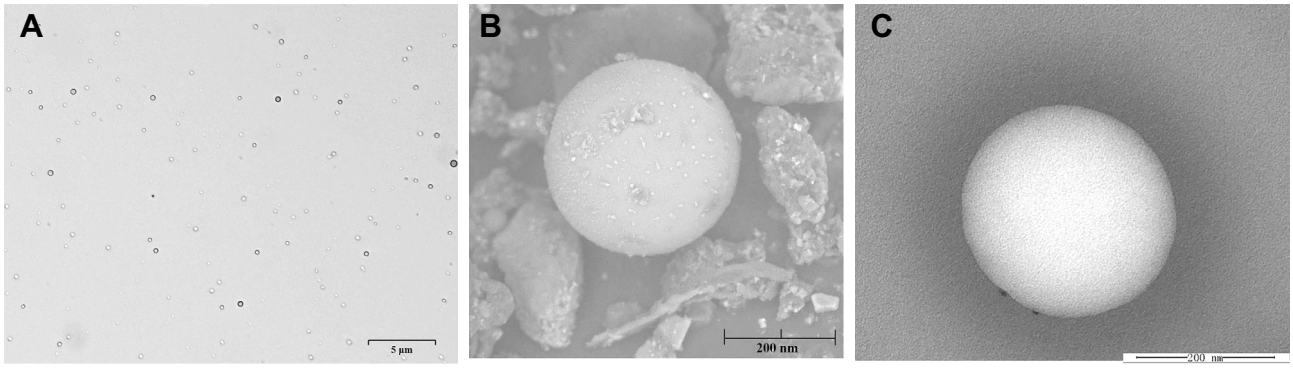

Figure 3 Morphology and structure of NDs. (**A**) The optical microscope (×1000) image (the scale bar represents 5 μm). (**B**) The SEM image (the scale bar represents 200 nm). (**C**) The TEM image (the scale bar represents 200 nm).

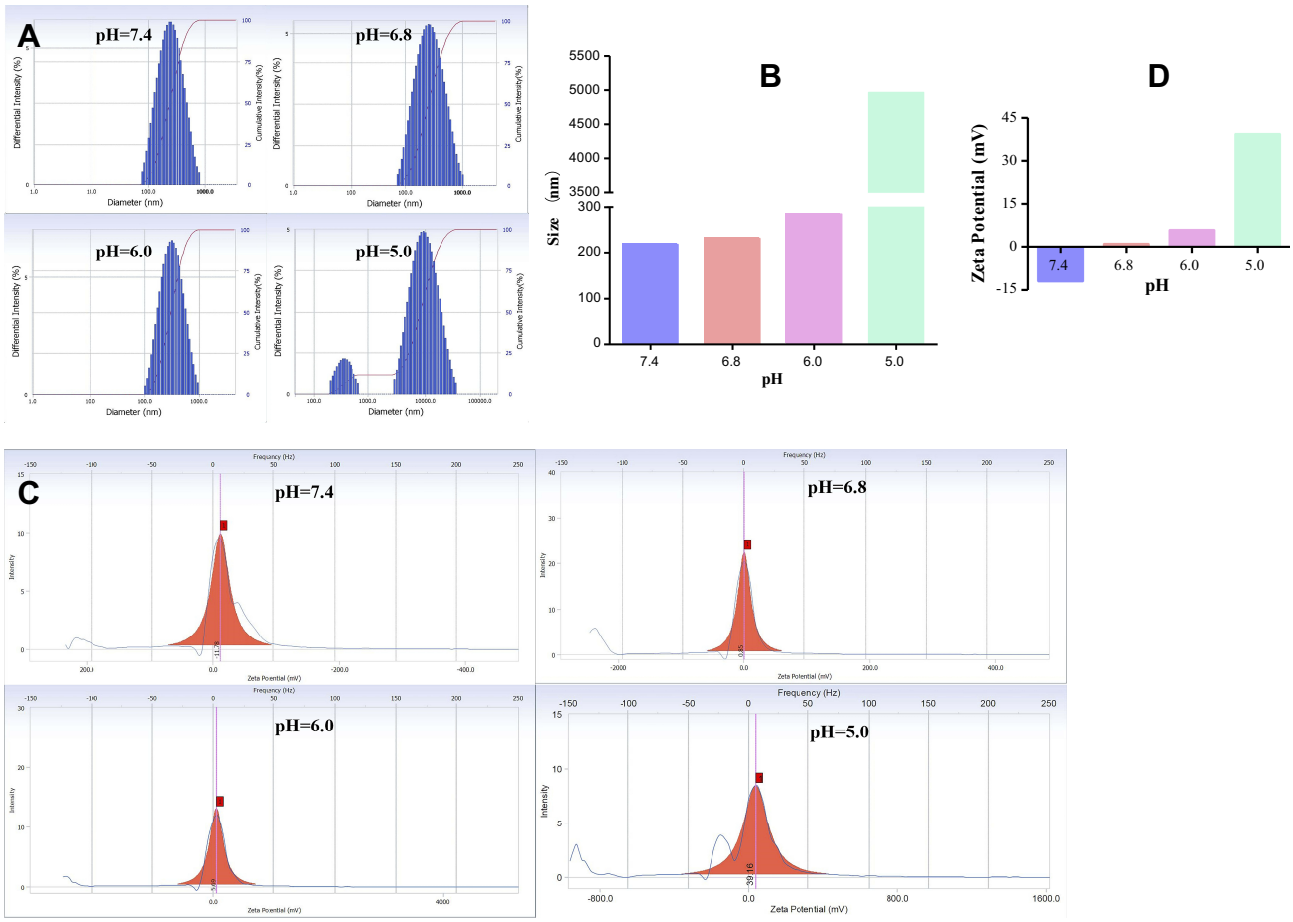

Figure 4 Characterization of NDs. (**A**) Size distribution of NDs at different pH conditions. (**B**) Size comparisons at different pH conditions. (**C**) Zeta potential of NDs at different pH conditions. (**D**) Zeta potential comparisons at different pH conditions.

average size (below 300 nm) with relatively narrow size distribution, as indicated by relatively low PDI value (less than 0.3, which indicates a relative homogeneous dispersion). However, if the pH value decreased to 5.0, the average size sharply increased to micron scale (4961.9 nm) with a high PDI value (1.199). This increase in sizes confirmed the aggregation of the NDs. Figure 4C and D showed the zeta potential changes with the decrement of pH values. From the results of the zeta potential analysis, NDs at pH 7.4 bore a negative charge

(−11.78 mV). When the pH condition was lower than 7.4, the zeta potentials conversed into positive charge and increased with the decrement of pH value. When the pH was 5.0, the zeta potential was even up to 39.16 mV.

Echogenicity of NDs as UCAs for Ultrasound Imaging

The phase change of NDs (the PFP entrapped in the NDs was evaporated) stimulated by surrounding temperature rise and ultrasound irradiation was observed with the ultrasonography in this study.

First, the relative greyscale imaging data of NDs at different temperature conditions (25°C and 37°C) and MI series (0.5, 0.9 and 1.2) are shown in Figure 5. Quantitative analysis revealed that there was a significant difference in greyscale intensity between NDs under different temperature conditions ($p<0.001$) and MI values ($p<0.001$). More echogenic NDs were observed under a higher surrounding temperature and MI set.

Second, NDs at 25°C, NDs at 37°C and, as a control, the degassed, deionized water were observed with the contrast mode of ultrasonography. NDs at both temperatures exhibited good echogenicity under the contrast mode, while the degassed, deionized water revealed no echogenicity (Figure 6A). The maximum contrast intensity of NDs at 25°C and 37°C was 34.4±0.52 dB, 41.2±0.77 dB, respectively ($p<0.001$) (Figure 6B). The "manual flash" contrast intensity of NDs at 25°C and 37°C was 50.18±0.08 dB, 52.84±0.11 dB, respectively ($p<0.001$) (Figure 6C). The ultrasound contrast intensities of the NDs at both 25°C and 37°C were continuously monitored for 10 min to analyze the time response contrast signal changes. The contrast intensities from 0 min to 10 min were plotted as a time course (Figure 6D). As seen, the contrast intensities from 0 min to 9 min of NDs at 37°C were significantly higher than those of NDs at 25°C. At the time point of 10 min, a same contrast intensity was observed between the two groups. In general, the contrast intensities of NDs at 25°C and 37°C both showed an obvious rise from 0 min to 2 min and then a slow fall from 2 min to 10 min. So the time point of 2 min was defined as the time of peak contrast intensity in this experiment. The survival ratios from 2 min to 10 min in the two groups were calculated (Table 1). The SRs of NDs at 25°C were larger than those of NDs at 37°C at all time points from 2 min to 10 min. The time to SR of 50% was both longer than 10 min for the two groups.

In vitro Cytotoxicity of NDs on PC3 Cell Line

Cytotoxicity assay is one of the assays highly preferred to find out the biocompatibility of the biomaterials. The cytotoxicity of NDs at decreasing concentrations (C1: 500 μg/mL; C2: 400 μg/mL; C3: 300 μg/mL; C4: 200 μg/mL; C5: 100 μg/mL; C6: 50 μg/mL; C7: 10 μg/mL; C8:5 μg/mL) was tested on PC3 cells (Figure 7A). The cell

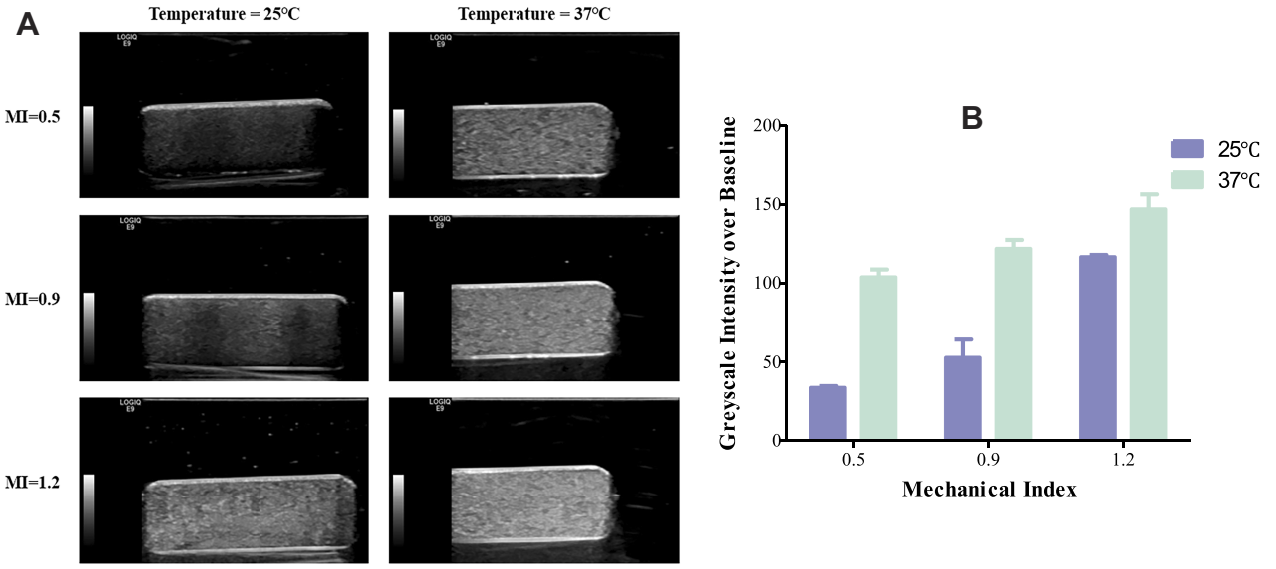

Figure 5 Capacity as UCAs for greyscale imaging in vitro. (**A**) The greyscale intensity of NDs under different MI and surrounding temperatures. (**B**) Greyscale intensity comparisons under different MI and surrounding temperatures.

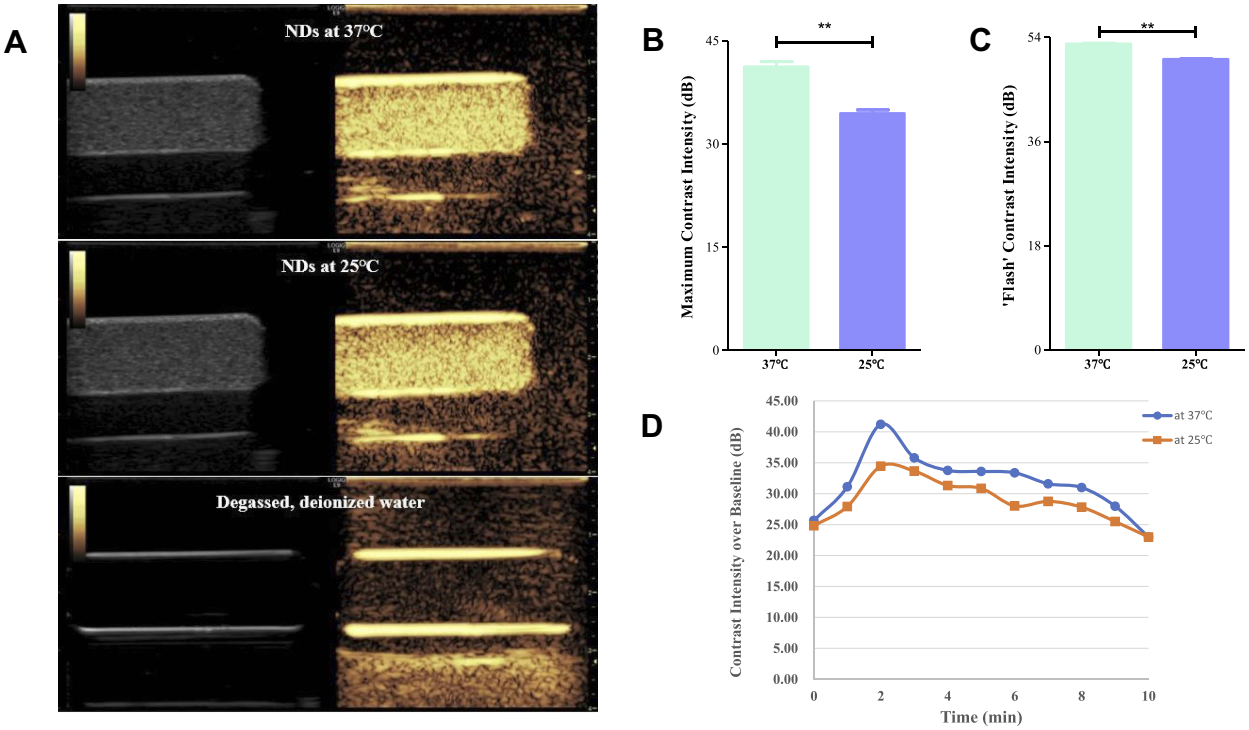

Figure 6 Capacity as UCAs for contrast enhancement in vitro. (**A**) The contrast images at the maximum contrast intensities of nanobubbles at 25°C and 37°C, the degassed, deionized water used as negative control. (**B**) Comparison of the maximum contrast intensities between 25°C and 37°C. **p<0.001. (**C**) Comparison of the "manual flash" contrast intensities between 25°C and 37°C. **p<0.001. (**D**) The SR curve of NDs at different time point.

viability incubated with ND concentration ≦100μg/mL was>94.34%±4.35%, and no significant changes in cell morphology were observed in comparison to the control cells, demonstrating low cytotoxicity of the NDs when the concentration was ≦100μg/mL.

Hemolysis Assay

Hemolysis assay is another one of the assays highly preferred to find out the biocompatibility of the biomaterials. Figure 7B shows the hemolysis assay image of NDs at decreasing concentrations (C1: 500μg/mL; C2: 400μg/mL; C3: 300μg/mL; C4: 200μg/mL; C5: 100μg/mL; C6: 50μg/mL; C7:10μg/mL; C8:5μg/mL). A concentration-dependent effect of NDs on hemolytic rate was observed in this experiment (Figure 7C). For the highest concentration, 500μg/mL, the hemolytic rate was 2.11%±2.38%, which indicated that the NDs could meet the needs of biomaterials (usually with a hemolytic rate ≦5%).

Preparation and Optimization of PTX-Loaded NDs

The protocols used to optimize the preparation of PTX-loaded NDs are described in Table 2. According to the results, the formula 3 generated a better LE (20.35%) and EE (91.58%), and it was selected for the optimum formula of PTX-loaded NDs.

pH-Responsive Drug Release from PTX-Loaded NDs

The PTX release properties were investigated at pH 7.4, 6.8, 6.0 and 5.0, which mimicked the conditions of normal tissue, tumor tissue, endosomal compartment and lysosome, respectively. In vitro drug release profile of PTX-loaded NDs at different conditions is shown in Figure 8. The in vitro drug release from PTX-loaded NDs exhibited an initial burst release followed by a sustained release over

Table 1 Survival Ratio (%) of NDs at Different Time Points

Temperature	2 Min*	3 Min	4 Min	5 Min	6 Min	7 Min	8 Min	9 Min	10 Min
25°C	100.00	97.74	90.94	89.61	81.36	83.51	80.78	74.04	66.72
37°C	100.00	86.85	81.90	81.51	80.98	76.66	75.21	67.88	55.75

Note: *Represented the time to peak contrast intensity.

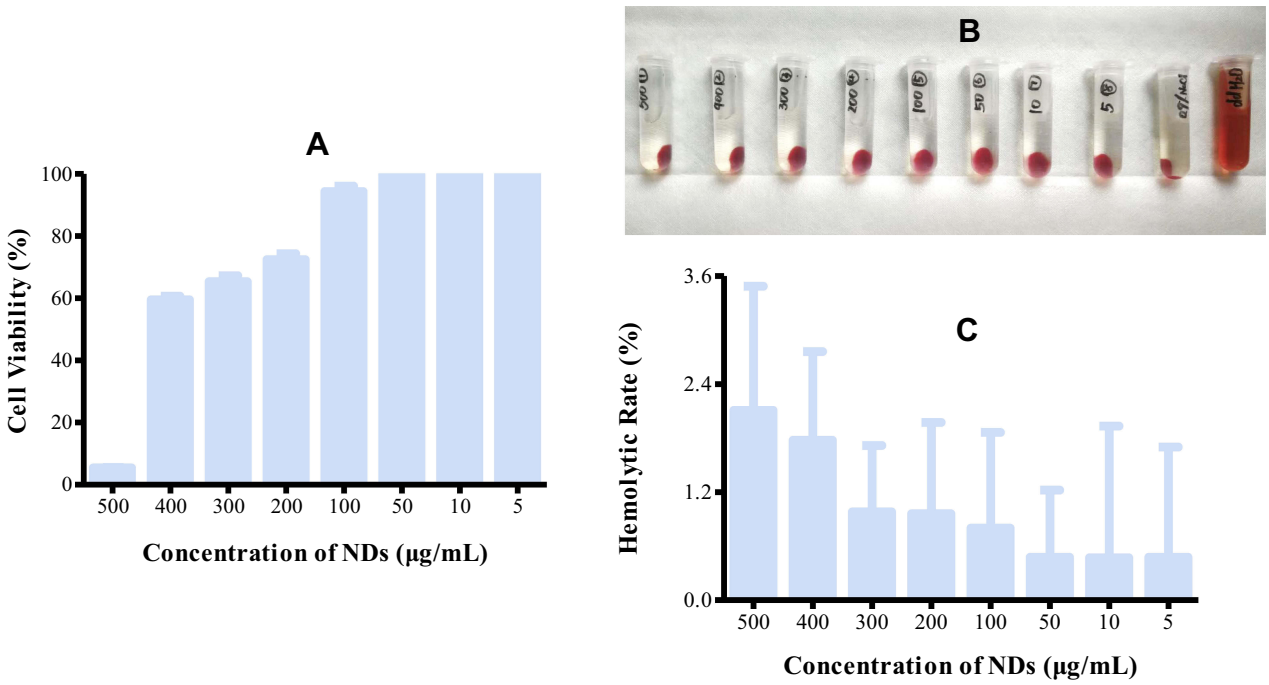

Figure 7 Biocompatibility evaluations of NDs. (**A**) Effect of different concentrations of NDs on PC3 cell viability evaluated by CCK-8 cytotoxicity assay. (**B**) In vitro hemolysis assay withNDs at different concentrations, using deionized water as positive control and 0.9% saline solution as negative control, respectively. (**C**) Hemolytic rate comparison between different concentrations of NDs.

a period of 72 h. The accumulative drug release percentages in 6 h were 18.52% at pH 7.4, 28.71% at pH 6.8, 32.92% at pH 6.0 and 38.71% at pH 5.0, respectively, and in 24 h were 56.15% at pH 7.4, 59.46% at pH 6.8, 66.49% at pH 6.0 and 87.64% at pH 5.0, respectively. Then, much slower release rates were observed in later time points. The drug release rates of the PTX-loaded NDs in this experiment were found pH-dependent. Higher accumulative drug release percentages were observed at lower pH values.

Cell Targeting Study of PTX-Loaded NDs on PC3 Cell Line

As shown in Figure 9, at pH 6.8, few PTX-loaded NDs were found in the region without cell attachment (the black oval region), while on the contrary, the most PTX-loaded NDs were observed near the cell membrane and even just a few entered into cells after 2 h (the red oval region). There was a significant difference in PTX-loaded ND distribution between the two regions. PTX-loaded NDs were successfully targeted to cells though charge attracts effect. The close cell-ND distance would contribute to efficiencies of cellular uptake, ultrasound sonoporation and drug delivery.[24]

Table 2 Formula Optimization of LE and EE of NDs

Formula	PTX (μg): CMC (μg)	LE (%)	EE (%)
1	750:9000	6.02	54.15
2	1125:9000	14.08	84.46
3	1500:9000	20.35	91.58

In vitro Cytotoxicity Assay

Figure 10A illustrates the results of cell viability of cells given different treatments. The control group cells served as control exhibiting 100% cell viability. There was a significant difference in cell viability among the 9 groups ($p<0.001$). The PTX-NDs+US+RT (6 Gy) group exhibited the most effective cytotoxicity among all the groups ($p<0.01$ in all cases), decreasing cell survival to 51.92% ±2.22%. The PTX+US+RT (6 Gy) group (63.91%±4.33%) showed more effective cytotoxicity than the PTX group (72.90%±3.83%), the RT (6 Gy) group (89.39±5.55%) and the RT (10 Gy) group (77.23%±3.95%) ($p<0.01$ in all cases). The NDs+US+RT (6 Gy) group decreased the cell survival to 81.72%±5.70% compared with the RT (6 Gy) group (89.39%±5.55%), but there was no significant difference between the two groups ($p>0.05$). There were 72.90%±3.83% and 85.05%±5.28% of cells that survived

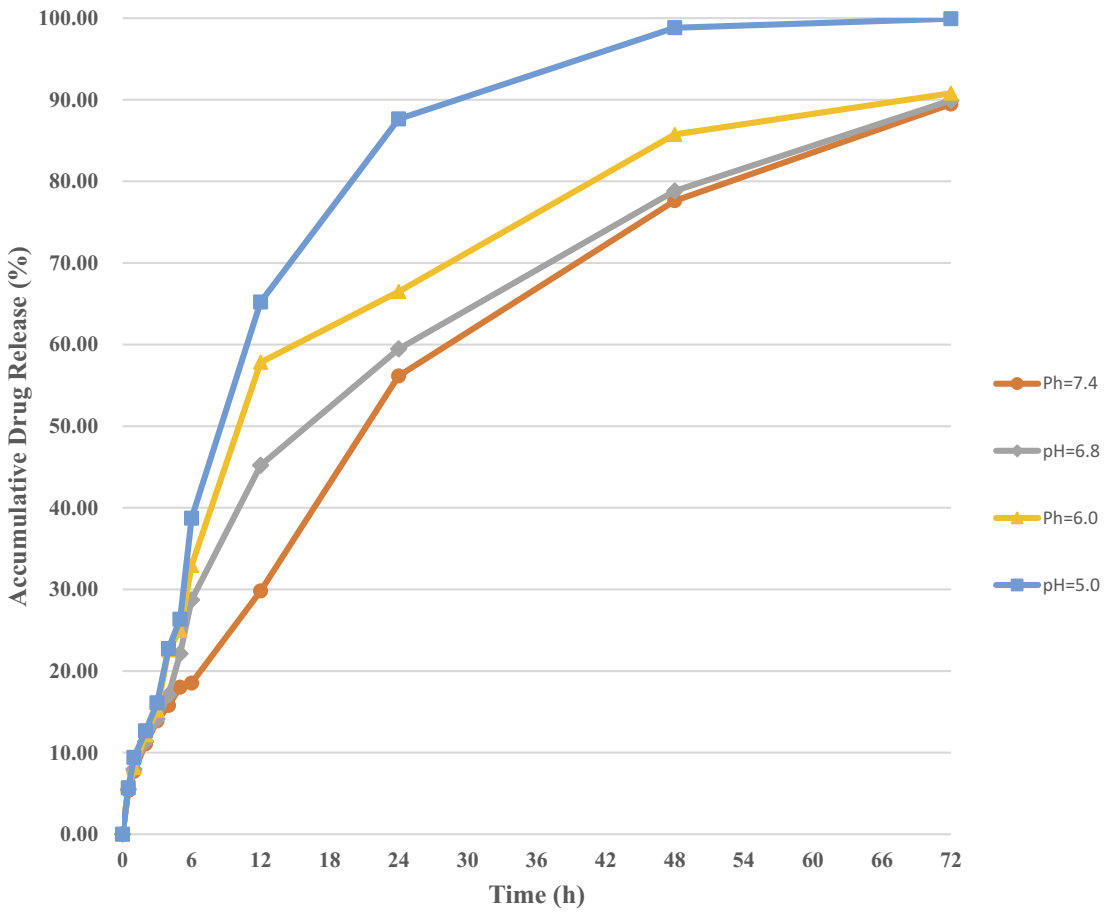

Figure 8 The drug release profile of the optimized PTX-loaded NDs at different pH conditions.

in the PTX group and PTX-NDs group ($p<0.01$), though the PTX amount was equal between the two groups. The ND group showed no obvious cytotoxicity with over 97.26%±4.22% of cell survival compared with the other groups ($p<0.05$ in all cases).

Flow Cytometry Assay

Quantitative analysis of Annexin V-FITC/PI double staining by flow cytometry was carried out to assess the early apoptosis (Q3), late apoptosis (Q2) and necrosis (Q1) rates in the 9 groups (Figure 10B). There was a significant difference in late apoptosis (Q2) rate ($p<0.001$) and necrosis (Q1) rate ($p<0.001$), while no significant difference in early apoptosis (Q3) rate ($p>0.05$) among the 9 groups. Consistent with the cytotoxicity assay, the PTX-NDs+US +RT (6 Gy) group showed significantly higher late apoptosis (Q2) rate (14.90%±2.03%) compared to the other groups ($p<0.05$ in all cases) except for the PTX+US+RT (6 Gy) group (12.87%±2.60%, $p>0.05$). The PTX+US+RT (6 Gy) group (12.87%±2.60%) showed significantly higher late apoptosis (Q2) rate than the RT (6 Gy) group (4.98% ±0.63%, $p<0.05$), but no significant difference was observed compared with the PTX group (10.02%±3.67%, $p<0.05$) and the RT (10 Gy) group (8.20%±2.83%, $p<0.05$). There was a significant difference in late apoptosis (Q2) rate between the PTX group and PTX-NDs group (10.02%±3.67% vs 5.48%±0.89%, $p<0.05$), though the PTX amount was equal. The NDs+US+RT (6 Gy) group increased the late apoptosis (Q2) rate compared with the RT (6 Gy) group (7.53%±1.19% vs 4.98%±0.63%), but there was no significant difference between the two groups ($p>0.05$).

Cell Migration Assay

Transwell migration results (Figure 10C) demonstrated that cells showed significantly different levels of migration among the 9 groups ($p<0.001$). Compared with the other groups, the PTX+US+RT (6 Gy) group reduced the

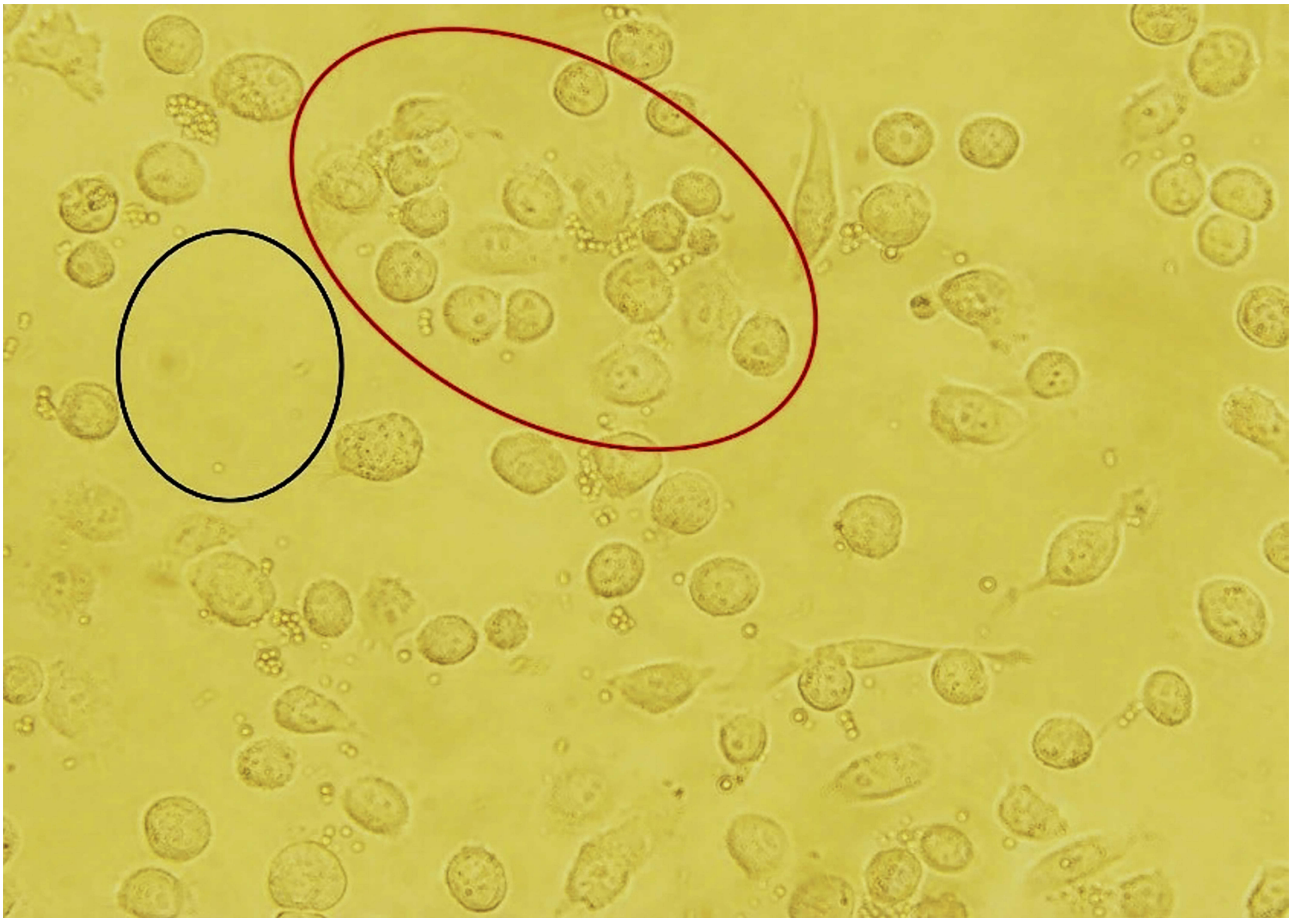

Figure 9 PTX-loaded NDs passively targeting on PC3 cell line in vitro. There was a significant difference in PTX-loaded ND distribution between regions with (red oval) and without (black oval) cell attachment.

migration numbers to different extents (103.33±7.64, $p<0.05$ in all cases) except for the PTX group (116.33 ±7.09, $p>0.05$) and the PTX+US+RT (6 Gy) group (112.00±7.55, $p>0.05$). The NDs+US+RT (6 Gy) group reduced the migration numbers compared with the RT (6 Gy) group (173.33±13.50 vs 177.00±6.25), but there was no significant difference between the two groups ($p>0.05$). There was a significant difference in migration numbers between the PTX group and PTX-NDs group (116.33 ±7.09 vs 147.67±4.62, $p<0.01$), though the PTX amount was equal.

Discussion

In recent decades, nanoscale UCAs have been received wide attention in various applications, especially in cancer management. Advanced nanoscale UCAs have been the focus of much research as enlightened theranostic agents, which allow not only tumor imaging but also precise and controlled drug/gene delivery.[25–28] However, very little was found in the literature on the question of developing nanoscale UCAs as sensitizers in RT and synergistic CRT. This inspires us to design a novel kind of nanoscale UCAs that can be responsive to the synergism of endogenous stimuli and exogeneous stimuli[29] to realize accurate and efficient CRT in tumor tissue but not in normal tissue. Focused on this idea, the pH- and ultrasound-responsive PFP-encapsulated, PTX-loaded CMC NDs were prepared in this study. Furthermore, the obtained results of this study were very encouraging, showing that the novel pH- and ultrasound-responsive PFP-encapsulated, PTX-loaded CMC NDs exhibited favorable characteristics for combined imaging and synergistic CRT.

To understand the radiosensitization effect of PTX-loaded NDs, the PC3 cells cultured without or with PTX, drug-free NDs and PTX-loaded NDs were exposed to varying dose of radiation with or without ultrasound irradiation. The results of a series of bioactivity/radiation assays, including CCK-8 assay, flow cytometry and

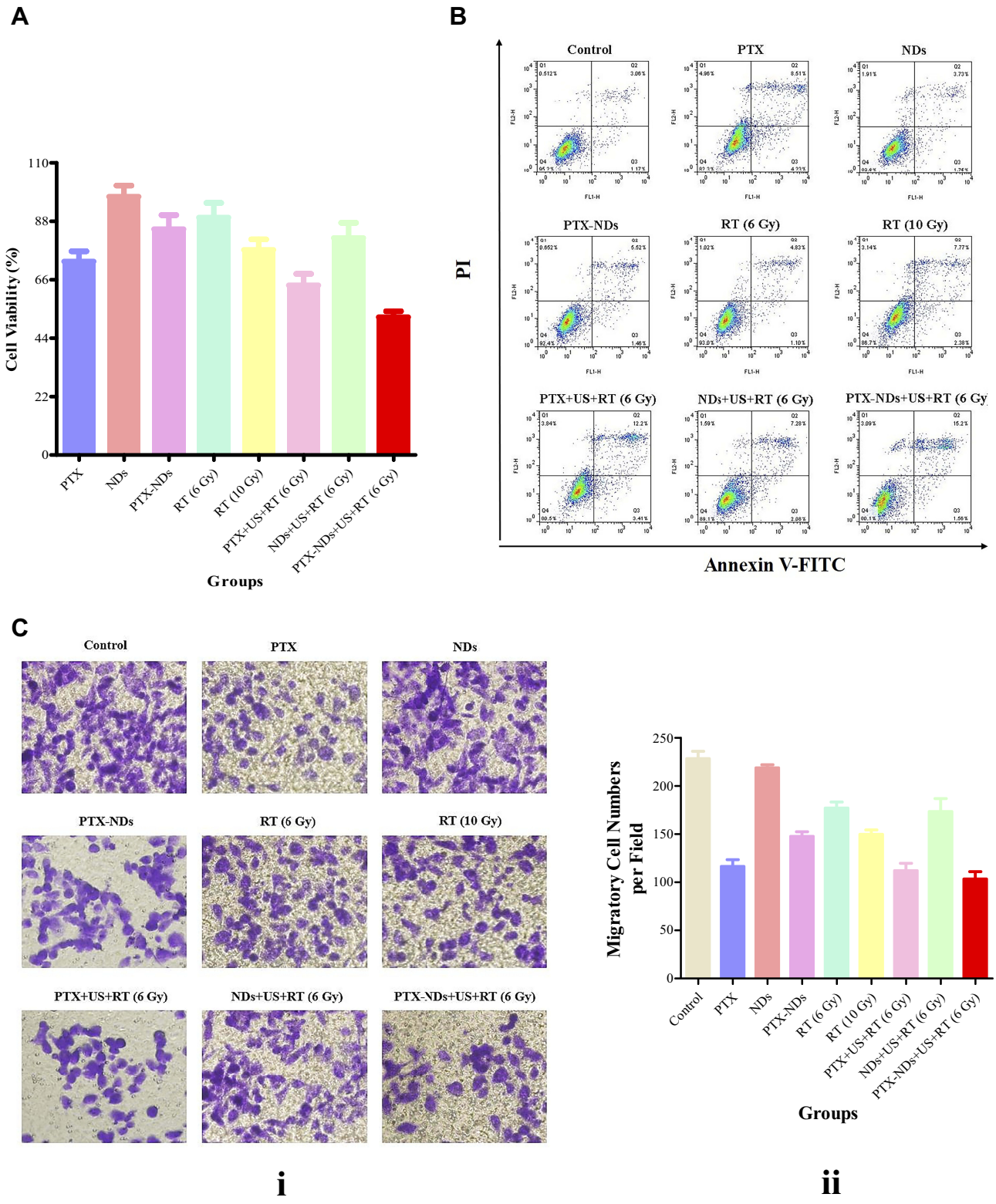

Figure 10 In vitro effect of PTX-loaded NDs on PC3 cells and their synergistic CRT efficiency. (**A**) The cytotoxicity assay results of different treatments. (**B**) Flow cytometric analysis of PC3 cells with different treatments. (**C**) Cell migration assay of PC3 cells with different treatments (i) and migratory cell comparisons between 9 groups (ii).

migration assay are shown in Figure 10. The PTX-loaded NDs combined ultrasound and RT significantly enhanced cell responses in CRT. What's more, the drug-free NDs combined ultrasound and RT also enhanced cell responses to a slight extent. There are several possible explanations for this result: First and most important, PTX released

from the NDs can sensitize tumor cells to radiation, which has been proven by several clinic and basic studies.[30,31] PTX-mediated radiosensitization is caused mainly by the stabilization of microtubules as a result of enhanced tubulin polymerization that leads to an accumulation of cells in the G2/M phase of cell cycle, which are known to be radiosensitive.[32] Second, the NDs combined ultrasound irradiation can mechanically perturb cell membranes, dysregulate biochemical signaling pathways of cell apoptosis, and additionally initiate tumor cell injury and lysis directly.[33,34] Early studies have discovered that the interaction of ultrasound with tissue can induce mechanical effects, chemical effects and thermal effects.[24] All these effects, which can be amplified by the combination use of UCAs, have been reported to be responsible for the above bioeffects. Thirdly, the NDs somewhat distribute O_2 to the hypoxic tumor cells, thus increasing the radiosensitivity of the cells.[35] In this study, PFP was selected as contrast agent material. PFP belongs to the categories of perfluorocarbon (PFC). Their high oxygen solubility, inertness and stability make them well suited for use as O_2 carriers and tumor radiosensitizers.[36,37] Though no additional O_2 was supplied, some O_2 was encapsulated in the NDs due to free O_2 diffusion during the high-speed homogenization/emulsion process.

For effectively enhancing the therapeutic efficiency and reducing the overall toxicity of synergistic CRT, the NDs in this study were developed to combine several necessary factors: Firstly, the average size of the NDs was below 300 nm with relatively narrow size distribution when the pH value was over 6.0 (Figure 4A and B). It is well known that the nanocarrier size significantly affects tumor/tissue penetration as well as biodistribution.[38] The appropriate size in this study could ensure the NDs extravasate from the leaky pores (380–780 nm) of vessels and accumulate in tumor parenchyma via EPR effect. Second, the pH-responsive features of the NDs indicated their ability to be used as DDSs. As is shown in Figure 4C and D, the zeta potential changes with the decrement of pH values. At pH 7.4, the NDs were negatively charged (−11.78 mV), avoiding the problem such as poor blood stability and cytotoxicity. But the NDs converted into positively charged under acidic conditions (pH≦6.8). The PTX-loaded NDs showed high pH-responsive charge-convertible capability, which demonstrated a much more rapid drug release under acidic conditions (tumor tissue) than under neutral conditions (normal tissue) (Figure 8) and a higher tumor cellular targeting (Figure 9). This phenomenon should be attributed to the amphoteric feature of the CMC, which is composed of both weak base groups ($-NH_2$) and weak acid groups (-COOH) linked by the backbone.[39] Of all the endogenous stimuli, pH alternation is more desirable than the other ones. The pH-responsive nanocarriers offer valuable capability for carrying therapeutic agents into the tumor tissue and the release of the encapsulated drugs could be triggered by the pH alternation. In accordance with the present results, previous studies have demonstrated that chitosan and its derivatives exhibit pH-dependent swelling properties.[40,41] The swelling properties result in the escape and release of loaded drugs from the cavities of particles. The protonated groups ($-NH_3^+$) of CMC generate a swelling osmotic pressure under acidic conditions and when these amino groups are deprotonated ($-NH_2$), the swelling osmotic pressure disappears under neutral conditions. Compared with the existing pH-responsive charge-convertible methods, which mostly achieved via complicated chemical processes,[42] CMC shows many promising advantages including its abundant natural precursor, excellent biocompatibility and biodegradability.[29] Third, the NDs were designed to accommodate PTX well in this study. As PTX is poorly soluble and stable in water, PTX-loaded nanocarriers were seldomly reported in the literature. PTX loading formula was investigated with different amounts of PTX and CMC in this study (Table 2). The highest EE of the PTX-loaded NDs was 91.85%. This result is in good consistency with other PTX nanocarriers.[43,44] The PTX-loaded NDs exhibited an initial burst release followed by a sustained release (Figure 8), which are also important for CRT. It is important to note that the drug release of the PTX-loaded NDs could be triggered by ultrasound irradiation through mechanical effect and thermal effect, which may be attributed to acoustic droplet vaporization of the NDs. The liquid-to-gas transition leads to the disruption of the ND assemblies and the subsequent release of their payloads.[45,46] Fourthly, the NDs demonstrated low cytotoxicity and hemocompatibility (Figure 6), which is particularly important when being used for biomedical purposes and facilitating potential clinical translation. The PTX-loaded NDs also exhibited a lower cytotoxicity than equivalent amount of PTX due to CMC encapsulation. What's more, their slow release of PTX may further enhance the efficacy of CRT.

The nanoscale UCAs with a strong ultrasound contrast enhancement effect and long contrast duration are conducive to effective synergistic CRT and assessment of therapeutic effects. To achieve this goal, PFP, which has a boiling point of 29.2°C, was used as the core the NDs. The PFP-encapsulated NDs in this study showed excellent ultrasound responses. Both greyscale imaging results (Figure 5) and contrast imaging results (Figure 6) indicated their ability to be used

as UCAs. Interestingly, the echogenicity of the NDs was found to increase initially with time and then slowly decreased. A possible explanation might be that the ultrasound irradiation induces the liquid-to-gas transition of the NDs. This transition could also be triggered by the surrounding temperature as the NDs at 37°C exhibited better echogenicity than at 25°C. The NDs showed a long and steady contrast ability with an SR of 50% longer than 10 min, which is enough to reach the target sites if used in vivo.

The above sections generally indicated the encouraging effect of the PTX-loaded NDs for the combined imaging and enhancing synergistic CRT efficiency. Although the results are promising, however, considerably more studies, such as a more detailed in vivo study, are necessary to fully evaluate the potential of the PTX-loaded NDs as a sensitizer in CRT. Also, further studies containing additional cell lines and more efficient radiosensitization agents are currently underway.

Conclusion

In summary, we have successfully developed a novel pH- and ultrasound-responsive PTX-loaded CMC NDs. These PTX-loaded NDs exhibited a high echogenicity, drug delivery ability and radiosensitization ability. We believe that the PTX-loaded NDs could be a feasible option for combined imaging and novel enhancing approach in synergistic CRT and hold great promise for future clinical translation.

Abbreviations

CRT, chemoradiotherapy; RT, radiotherapy; DDS, drug delivery system; EPR, enhanced permeability and retention; NPs, nanoparticles; UCAs, ultrasound contrast agents; PTX, paclitaxel; CMC, carboxymethyl chitosan; PFP, perfluoropentane (C_5F_{12}); NDs, nanodroplets; FBS, fetal bovine serum; PBS, phosphate saline buffer; CCK-8, cell counting kit-8; LE, loading efficiency; EE, encapsulation efficiency; SR, survival ratio; ROI, region of interest; PDI, polydispersity index; SEM, scanning electron microscopy; TEM, transmission electron microscopy; MI, mechanical index.

Acknowledgment

This work was financially supported by the National Natural Science Foundation of China (NO. 81771843), the Science and Technology Developing Program of Shandong Provincial Government of China (2017GSF18107).

Disclosure

The authors declare no conflicts of interest in this work.

References

1. Seiwert TY, Salama JK, Vokes EE. The concurrent chemoradiation paradigm - general principles. *Nat Clin Pract Oncol*. 2007;4(2):86–100. doi:10.1038/ncponc0714
2. Brunner TB. The rationale of combined radiotherapy and chemotherapy - joint action of Castor and Pollux. *Best Pract Res Clin Gastroenterol*. 2016;30(4):515–528. doi:10.1016/j.bpg.2016.07.002
3. Sun Y, Li WF, Chen N, et al. Induction chemotherapy plus concurrent chemoradiotherapy versus concurrent chemoradiotherapy alone in locoregionally advanced nasopharyngeal carcinoma: a Phase 3, multicentre, randomised controlled trial. *Lancet Oncol*. 2016;17(11):1509–1520. doi:10.1016/S1470-2045(16)30410-7
4. Kawamoto T, Shikama N, Oshima M, et al. Safety of radiotherapy with concurrent docetaxel in older patients with esophageal cancer. *J Geriatr Oncol*. 2019. doi:10.1016/j.jgo.2019.08.009
5. Kanzaki R, Ose N, Funaki S, et al. The outcomes of induction chemoradiotherapy followed by surgery for clinical T3-4 non-small cell lung cancer. *Technol Cancer Res Treat*. 2019;18:1533033819871327. doi:10.1177/1533033819871327
6. Brunner TB, Seufferlein T. Pancreatic cancer chemoradiotherapy. *Best Pract Res Clin Gastroenterol*. 2016;30(4):617–628. doi:10.1016/j.bpg.2016.08.001
7. Cooper BT, Sanfilippo NJ. Concurrent chemoradiation for high-risk prostate cancer. *World J Clin Oncol*. 2015;6(4):35–42. doi:10.5306/wjco.v6.i4.35
8. Fu ZZ, Li K, Peng Y, et al. Efficacy and toxicity of different concurrent chemoradiotherapy regimens in the treatment of advanced cervical cancer: a network meta-analysis. *Medicine (Baltimore)*. 2017;96(2):e5853. doi:10.1097/MD.0000000000005853
9. Shah BA, Qureshi MM, Logue JM, et al. Assessing cumulative acute toxicity of chemoradiotherapy in head and neck cancer with or without induction chemotherapy. *Am J Otolaryngol*. 2017;38(4):456–461. doi:10.1016/j.amjoto.2017.04.004
10. Werner ME, Foote MB, Wang AZ. Chemoradiotherapy of human tumors: novel approaches from nanomedicine. *Curr Pharm Des*. 2012;18(19):2830–2837. doi:10.2174/138161212800626229
11. Bahrami B, Hojjat-Farsangi M, Mohammadi H, et al. Nanoparticles and targeted drug delivery in cancer therapy. *Immunol Lett*. 2017;190:64–83. doi:10.1016/j.imlet.2017.07.015
12. Liu Y, Miyoshi H, Nakamura M. Nanomedicine for drug delivery and imaging: a promising avenue for cancer therapy and diagnosis using targeted functional nanoparticles. *Int J Cancer*. 2007;120(12):2527–2537. doi:10.1002/(ISSN)1097-0215
13. Xin Y, Huang Q, Tang JQ, et al. Nanoscale drug delivery for targeted chemotherapy. *Cancer Lett*. 2016;379(1):24–31. doi:10.1016/j.canlet.2016.05.023
14. Beik J, Khademi S, Attaran N, et al. A nanotechnology-based strategy to increase the efficiency of cancer diagnosis and therapy: folate-conjugated gold nanoparticles. *Curr Med Chem*. 2017;24(39):4399–4416. doi:10.2174/0929867324666170810154917
15. Ding C, Li Z. A review of drug release mechanisms from nanocarrier systems. *Mater Sci Eng C Mater Biol Appl*. 2017;76:1440–1453. doi:10.1016/j.msec.2017.03.130
16. Das RP, Gandhi VV, Singh BG, et al. Passive and active drug targeting: role of nanocarrier in rational design of anticancer formulations. *Curr Pharm Des*. 2019;25(28):3034–3056. doi:10.2174/1381612825666190830155319
17. Tian J, Min Y, Rodgers Z, et al. Co-delivery of paclitaxel and cisplatin with biocompatible PLGA-PEG nanoparticles enhances chemoradiotherapy in non-small cell lung cancer models. *J Mater Chem B*. 2017;5(30):6049–6057. doi:10.1039/C7TB01370A
18. Mirrahimi M, Khateri M, Beik J, et al. Enhancement of chemoradiation by co-incorporation of gold nanoparticles and cisplatin into alginate hydrogel. *J Biomed Mater Res B Appl Biomater*. 2019;107(8):2658–2663. doi:10.1002/jbm.v107.8

19. Li H, Gan S, Feng ST, et al. Nano-sized ultrasound contrast agents for cancer therapy and theranostics. *Curr Pharm Des*. 2017;23(35):5403–5412. doi:10.2174/1381612823666170710120631
20. Deshpande N, Needles A, Willmann JK. Molecular ultrasound imaging: current status and future directions. *Clin Radiol*. 2010;65(7):567–581. doi:10.1016/j.crad.2010.02.013
21. Hui L, Chen Y. Tumor microenvironment: sanctuary of the devil. *Cancer Lett*. 2015;368(1):7–13. doi:10.1016/j.canlet.2015.07.039
22. Staedler D, Passemard S, Magouroux T, et al. Cellular uptake and biocompatibility of bismuth ferrite harmonic advanced nanoparticles. *Nanomedicine*. 2015;11(4):815–824. doi:10.1016/j.nano.2014.12.018
23. Xu J, Ma L, Liu Y, et al. Design and characterization of antitumor drug paclitaxel-loaded chitosan nanoparticles by W/O emulsions. *Int J Biol Macromol*. 2012;50(2):438–443. doi:10.1016/j.ijbiomac.2011.12.034
24. Lentacker I, De Cock I, Deckers R, et al. Understanding ultrasound induced sonoporation: definitions and underlying mechanisms. *Adv Drug Deliv Rev*. 2014;72:49–64. doi:10.1016/j.addr.2013.11.008
25. Zhang J, Chen Y, Deng C, et al. The optimized fabrication of a novel nanobubble for tumor imaging. *Front Pharmacol*. 2019;10:610. doi:10.3389/fphar.2019.00610
26. Nittayacharn P, Yuan HX, Hernandez C, et al. Enhancing tumor drug distribution with ultrasound-triggered nanobubbles. *J Pharm Sci*. 2019;108(9):3091–3098. doi:10.1016/j.xphs.2019.05.004
27. Suzuki R, Oda Y, Omata D, et al. Tumor growth suppression by the combination of nanobubbles and ultrasound. *Cancer Sci*. 2016;107(3):217–223. doi:10.1111/cas.12867
28. Negishi Y, Endo-Takahashi Y, Maruyama K. Gene delivery systems by the combination of lipid bubbles and ultrasound. *Drug Discov Ther*. 2016;10(5):248–255. doi:10.5582/ddt.2016.01063
29. Fathi M, Sahandi Zangabad P, Majidi S, et al. Stimuli-responsive chitosan-based nanocarriers for cancer therapy. *Bioimpacts*. 2017;7(4):269–277. doi:10.15171/bi.2017.32
30. Lin H, Chen Y, Shi A, et al. Phase 3 randomized low-dose paclitaxel chemoradiotherapy study for locally advanced non-small cell lung cancer. *Front Oncol*. 2016;6:260. doi:10.3389/fonc.2016.00260
31. Gabikian P, Tyler BM, Zhang I, et al. Radiosensitization of malignant gliomas following intracranial delivery of paclitaxel biodegradable polymer microspheres. *J Neurosurg*. 2014;120(5):1078–1085. doi:10.3171/2014.1.JNS13235
32. Kunos CA, Stefan T, Jacobberger JW. Cabazitaxel-induced stabilization of microtubules enhances radiosensitivity in ovarian cancer cells. *Front Oncol*. 2013;3:226. doi:10.3389/fonc.2013.00226
33. El Kaffas A, Czarnota GJ. Biomechanical effects of microbubbles: from radiosensitization to cell death. *Future Oncol*. 2015;11(7):1093–1108. doi:10.2217/fon.15.19
34. Czarnota GJ. Ultrasound-stimulated microbubble enhancement of radiation response. *Biol Chem*. 2015;396(6–7):645–657. doi:10.1515/hsz-2014-0297
35. Eisenbrey JR, Shraim R, Liu JB, et al. Sensitization of hypoxic tumors to radiation therapy using ultrasound-sensitive oxygen microbubbles. *Int J Radiat Oncol Biol Phys*. 2018;101(1):88–96. doi:10.1016/j.ijrobp.2018.01.042
36. Xu X, Song R, He M, et al. Microfluidic production of nanoscale perfluorocarbon droplets as liquid contrast agents for ultrasound imaging. *Lab Chip*. 2017;17(20):3504–3513. doi:10.1039/C7LC00056A
37. Sheeran PS, Dayton PA. Improving the performance of phase-change perfluorocarbon droplets for medical ultrasonography: current progress, challenges, and prospects. *Scientifica (Cairo)*. 2014;2014:579684. doi:10.1155/2014/726179
38. He C, Hu Y, Yin L, Tang C, Yin C. Effects of particle size and surface charge on cellular uptake and biodistribution of polymeric nanoparticles. *Biomaterials*. 2010;31(13):3657–3666. doi:10.1016/j.biomaterials.2010.01.065
39. Fonseca-Santos B, Chorilli M. An overview of carboxymethyl derivatives of chitosan: their use as biomaterials and drug delivery systems. *Mater Sci Eng C Mater Biol Appl*. 2017;77:1349–1362. doi:10.1016/j.msec.2017.03.198
40. Unsoy G, Yalcin S, Khodadust R, et al. Chitosan magnetic nanoparticles for pH responsive Bortezomib release in cancer therapy. *Biomed Pharmacother*. 2014;68(5):641–648. doi:10.1016/j.biopha.2014.04.003
41. Rajan M, Murugan M, Ponnamma D, et al. Poly-carboxylic acids functionalized chitosan nanocarriers for controlled and targeted anti-cancer drug delivery. *Biomed Pharmacother*. 2016;83:201–211. doi:10.1016/j.biopha.2016.06.026
42. Deirram N, Zhang C, Kermaniyan SS, et al. pH-responsive polymer nanoparticles for drug delivery. *Macromol Rapid Commun*. 2019;40(10):e1800917. doi:10.1002/marc.201800917
43. Almeida A, Silva D, Goncalves V, et al. Synthesis and characterization of chitosan-grafted-polycaprolactone micelles for modulate intestinal paclitaxel delivery. *Drug Deliv Transl Res*. 2018;8(2):387–397. doi:10.1007/s13346-017-0357-8
44. Li J, Yuan Z, Yan M, et al. pH-sensitive micelles loaded paclitaxel using carboxymethyl chitosan-palmitic acid mediated by cRGD. *Acta Pharmaceutica Sinica*. 2016;51(4):642–649.
45. Abed Z, Khoei S, Ghalandari B, et al. The measurement and mathematical analysis of 5-Fu release from magnetic polymeric nanocapsules, following the application of ultrasound. *Anticancer Agents Med Chem*. 2018;18(3):438–449.
46. Beik J, Abed Z, Ghadimi-Daresajini A, et al. Measurements of nanoparticle-enhanced heating from 1MHz ultrasound in solution and in mice bearing CT26 colon tumors. *J Therm Biol*. 2016;62(Pt A):84–89. doi:10.1016/j.jtherbio.2016.10.007